

# Anti-microRNA-378a Enhances Wound Healing Process by Upregulating Integrin Beta-3 and Vimentin

Haoran Li<sup>1,2</sup>, Leslie Chang<sup>1,2</sup>, William W Du<sup>1,2</sup>, Shaan Gupta<sup>1,2</sup>, Azam Khorshidi<sup>1,2</sup>, Michael Sefton<sup>1,2</sup> and Burton B Yang<sup>1,2</sup>

<sup>1</sup>Sunnybrook Research Institute, Sunnybrook Health Sciences Centre, Toronto, Ontario, Canada; <sup>2</sup>Department of Laboratory Medicine and Pathobiology, University of Toronto, Toronto, Ontario, Canada

Delayed or impaired wound healing is a major public health issue worldwide, especially in patients with diabetes mellitus and vascular atherosclerosis. MicroRNAs have been identified as key regulators of wound healing. Here, we show that miR-Pirate378a transgenic mice (and thus have inhibited miR-378a-5p function) display enhanced wound healing. Expression of vimentin and  $\beta 3$  integrin, two important modulators of wound healing, is markedly elevated in the transgenic mice. MiR-Pirate378a-transfected cells display greater mobility during migration assays, which was hypothesized to be due to the upregulation of vimentin and  $\beta 3$  integrin. Both molecules were confirmed to be targets of miR-378a, and thus their expression could be rescued by miR-Pirate378a. Overexpression of vimentin also contributed to fibroblast differentiation, and upregulation of  $\beta 3$  integrin was responsible for increased angiogenesis. Mice treatment with miR-Pirate378a-conjugated nanoparticles displayed enhanced wound healing. Thus, we have demonstrated that knockdown of miR-378a increased the expression of its target proteins, vimentin, and  $\beta 3$  integrin, which accelerated fibroblast migration and differentiation *in vitro* and enhanced wound healing *in vivo*.

Received 9 December 2013; accepted 12 June 2014; advance online publication 5 August 2014. doi:10.1038/mt.2014.115

## INTRODUCTION

As the largest organ of human body, the skin acts as the first line of protection against environmental hazards. Dysfunctions of the skin's wound healing process can result in cosmetic problems, metabolic disorders, and lethal infection. Cutaneous wound healing is a complex biological process which consists of hemostasis, inflammation, reepithelization, vascularization, and tissue remodeling. Delayed or impaired wound healing has been a major public health issue worldwide, especially in patients with diabetes mellitus and vascular atherosclerosis. It is estimated that as many as 15% of the population with diabetes are at the risk of nonhealing ulcers, and that the cost of treating these patients is about 10 billion dollars each year.<sup>1</sup>

The human genome encodes over 100,048 microRNAs (miRNAs), and some are involved in the tissue repair processes such as inflammation, angiogenesis, cell differentiation, and migration.<sup>2</sup> Although dysregulation of miRNAs are often shown to be related with compromised wound healing, the intrinsic mechanisms remain to be fully understood.

There are two main approaches to studying miRNA function: gain-of-function and loss-of-function tests. Gain-of-function studies are performed by introducing a particular miRNA molecule into cells or animal genomes, and observing the biological phenotype.<sup>3,4</sup> By contrast, loss-of-function studies can be used to silence a miRNA's functions, thereby evaluating the corresponding changes *in vitro* and *in vivo*. This can be achieved by noncoding transcripts<sup>5-7</sup> or specific miRNA sponges.<sup>8,9</sup>

Reverse genetic approaches that inhibit miRNA function have widely been used to facilitate functional studies. To date, many efforts have been made to successfully silence miRNAs. The development of anti-miRNA oligonucleotide (AMO) technology has opened up vast opportunities for miRNA silencing. Developmental defects in *Drosophila* embryos were observed by injecting antisense oligonucleotides to suppress miR-13.<sup>10</sup> However, unmodified AMOs, such as the one used in this study, can be degraded by nucleotidase, limiting its application *in vivo*.<sup>10</sup> Chemical modifications of AMOs may confer resistance to degradation and increase target affinity. For example, 2'-O-methyl oligoribonucleotides were shown to specifically inactivate miRNA-protein complexes in cultured human cells.<sup>11</sup> These modified AMOs display higher melting temperature and greater liver microsomal stability when bound to miRNA than their unmodified counterparts. Locked nucleic acids are another modification used to optimize the chemical structure of AMOs, significantly increasing target affinity by introducing locked nucleic acids substitutions into AMO backbones.<sup>12</sup> Although the use of AMOs may be a good strategy for therapeutically inhibiting miRNAs, challenges in reaching sufficient transfection rates remain. Therefore, the endogenous expression of antisense miRNAs builds a more stable system for comprehensive studies *in vivo*. The first endogenous antisense miRNA (anti-miRNA) was reported by Carè *et al.*<sup>13</sup> They developed a construct with a 3'-untranslated region designed to bind cellular miR-133, and found that a single infusion of this

Correspondence: Burton B Yang, S110, S-Wing Research Building, Sunnybrook Health Sciences Centre, 2075 Bayview Ave, Toronto M4N 3M5 Canada. E-mail: byang@sri.utoronto.ca

antagomir construct led to cardiac hypertrophy in mouse.<sup>13</sup> To enhance inhibition potency, anti-miRNA sponges were made by inserting multiple tandem miRNA binding sites into vectors with a cytomegalovirus promoter. These stably expressed sponges can also be used to block an entire miRNA family, which contain identical seed sequences.<sup>8,9</sup> This is advantageous over traditional gene knock-out technologies, which have been shown to be less efficient in silencing multiple genomic loci within one miRNA family (such as those in the let-7 and miR-17–92 clusters). Therefore, the use of stably integrated anti-miRNA sponges provides a new tool for studying miRNA function in animal models.

Our previous studies revealed that microRNA-378a (miR-378a) plays a role in modulating cell migration and differentiation *in vitro*, and we further demonstrated that the function of miR-378a was subject to complex regulation in differentiated MC3T3 cells.<sup>14,15</sup> This led us to investigate the role of miR-378a in tissue remodeling, using a miR-Pirate378a (anti-miR-378a) construct.

## RESULTS

### Enhanced wound healing in miR-Pirate378a transgenic mice

CD1 miR-Pirate378a (anti-miR-378a) transgenic mice were generated by microinjection of transgene fragments into fertilized zygotes (Figure 1a). Newborns were screened for the presence of the miR-Pirate378a sequence and positive samples were interbred with CD1 wild type mice to obtain F1 generation. Tail clips were used for PCR genotyping to identify positive transgenic mice. Real-time PCR was employed to confirm the miR-378a and miR-Pirate378a levels. The sequences of primers used in this study are provided in Supplementary Information (Supplementary Figure S1a). We previously showed that the miR-Pirate378a transcript could interfere with miR-378a by targeting precursor miR-378a as well as arresting mature miRNA.<sup>16</sup> Detecting the levels of miR-Pirate378a allowed us to estimate misprocessing of endogenous miR-378a. We detected high levels of truncated miR-378a as compared with wild type mice (Supplementary Figure 1b). It was anticipated that the misprocessed miR-378a could not be recognized by Dicer, since it lacked the intact “seed” regions.<sup>16</sup> As a result, mature miR-378a expression was repressed due to the introduction of miR-Pirate378a fragments.

MiRNAs function to maintain physical homeostasis, and are also subject to the regulation of other signaling networks.<sup>17</sup> For example, expression of miR-378a changes during the differentiation of MC3T3 cells.<sup>15</sup> We previously demonstrated that vimentin, one of the cytoskeletal proteins which are crucial to wound healing, could mediate miR-378a's expression and function.<sup>14,18</sup> To study how miR-378a influences tissue repair and wound healing, miR-Pirate378a transgenic and wild type mice were subject to a cervical dermal punch biopsy, which left full-thickness excisional wounds around 5 mm on both sides of the neck. One week after wounding, miR-Pirate378a transgenic mice showed enhanced healing as compared to the wild-type mice (Figure 1c). Studies have shown that genders and sex steroids might impact tissue repair and regeneration.<sup>19</sup> In our studies, both male and female transgenic mice displayed accelerated wound healing. The difference in wound area between two groups was statistically significant after 6 days (Figure 1d). Measurements of wound area

revealed that the ratios of unhealed space (Day 6: Day 1) were significantly smaller in miR-Pirate378a group than that in the wild-type mice (Figure 1d).

On the seventh day, tissues of wound area were biopsied for histological examination and immunohistochemistry staining. Wound healing is driven by myofibroblast migration and transition, which is marked by expression of alpha-smooth muscle actin.<sup>20</sup> Confocal microscope showed that there was increased alpha-smooth muscle actin expression in the miR-Pirate378a transgenic mice, as compared to that in wild type (Figure 2a). We also found that there were more new blood vessels generated *in situ* in the miR-Pirate378a mice, as evaluated by CD34 levels (Figure 2b). Nevertheless, there was no apparent difference in epithelial cell proliferation in both groups, as indicated by BrdU and Ki67 staining (Figure 2b). All negative controls were conducted and one typical photo is provided in the figure. The numbers of stained blood vessels and cells were counted for quantitation (Figure 2c).

### MiR-Pirate378a accelerates fibroblasts migration, differentiation, and tube formation

Fibroblasts are known to be essential in tissue repair. They move to the wound area upon wound formation and synthesize collagen together with other extracellular matrix, generating the force required to contract the wound. To study the function of miR-378a on fibroblast activities, NIH/3T3 cells were stably transfected with plasmids containing green fluorescent protein as a mock control, the pre-miR-378a coding sequence, or miR-Pirate378a fragments. Real-time PCR was used to confirm the expression of miR-378a in transfected cells. There was an elevation of misprocessed miR-378a in cells overexpressing miR-Pirate378a (Figure 3a). As a result, miR-378a-transfected cells expressed higher levels of mature miR-378a-5p, whereas miR-Pirate378a-transfected cells expressed significantly lower levels of miR-378a-5p than the control (Figure 3a).

We performed a number of cell activity assays to test the effects of miR-378a on cell biology associated with wound repair. In cell migration assay, the miR-Pirate378a-transfected cells showed a greater ability to migrate, as compared to miR-378a-transfected and green fluorescent protein-control cells (Figure 3b, Supplementary Figure S1b). The locomotion of fibroblasts during wound healing includes migration as well as deformation. Thus, transwell migration assay was performed to test both functions. After being placed above a cell permeable membrane for 8 hours, more miR-Pirate378a-transfected cells migrated through microspores of the membrane (Figure 3c, Supplementary Figure S1c). In cell adhesion assay, NIH/3T3 cells were incubated on Petri dish for 2 hours to test adhesion ability. It was found that more miR-Pirate378a-transfected cells were able to attach to the surface of Petri dish (Figure 3d, Supplementary Figure S1d). By coculturing NIH/3T3 cells with YPEN endothelial cells, the cells formed tube-like structures, mimicking angiogenesis. There were more tube-like structures formed in miR-Pirate378a-transfected cells, while miR-378a expression largely inhibited tube formation (Supplementary Figure S1e).

Tissue repair requires the differentiation of fibroblasts into functional mature cells. Thus, differentiation of fibroblasts is



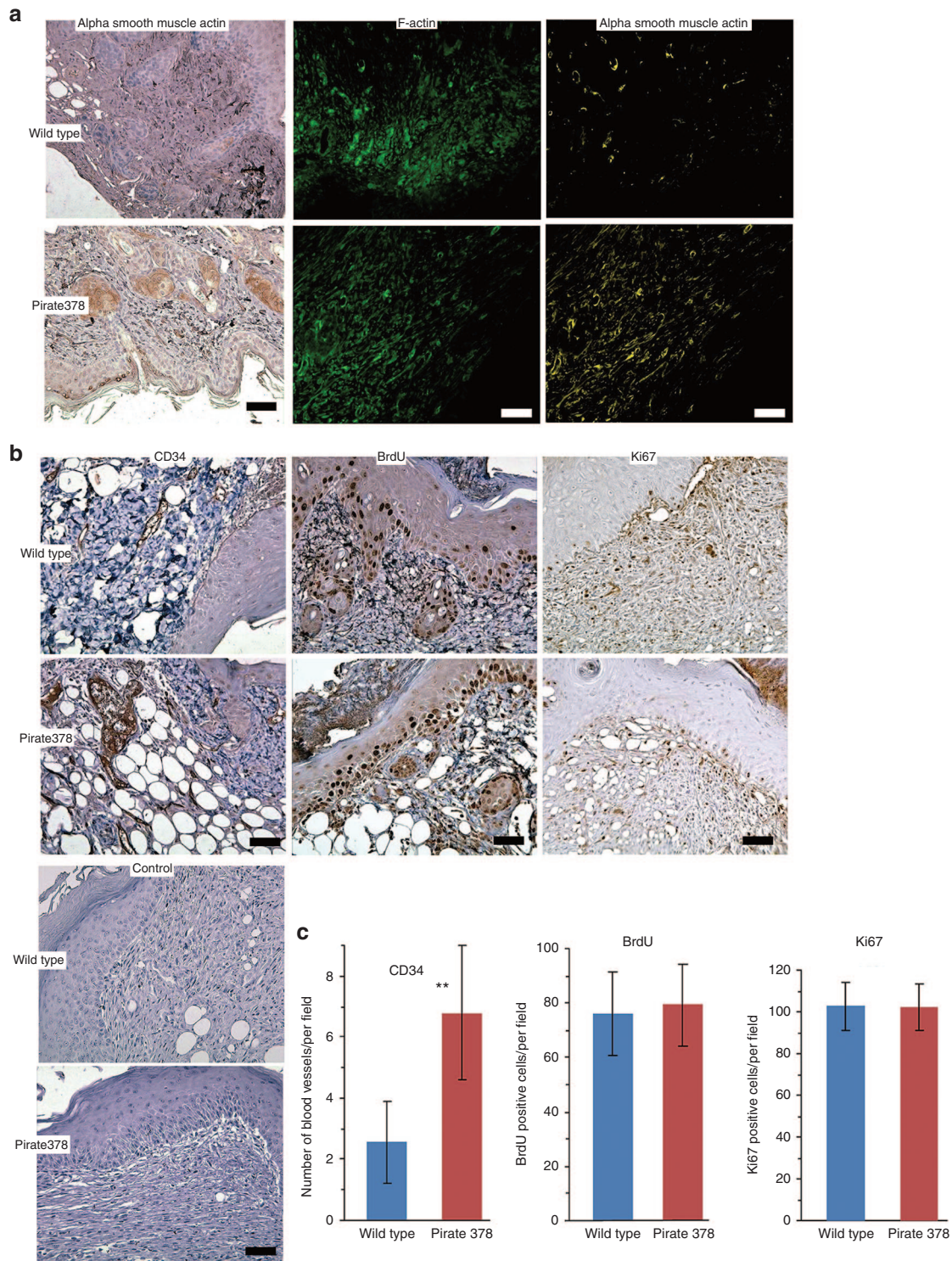


**Figure 2** MiR-Pirate378a increases CD34 expression. **(a)** Wound tissue samples were subject to immunohistochemistry analysis. Expressions of alpha smooth muscle actin increased in miR-Pirate378a transgenic mice samples. There was no difference in F-actin expression between these two groups. Scale bar = 50  $\mu$ m. **(b)** Wound tissue samples were subject to immunohistochemistry analysis. Expressions of CD34 increased in miR-Pirate378a transgenic mice samples. There was no difference in BrdU and Ki67 expression between these two groups. Scale bar = 50  $\mu$ m. **(c)** The numbers of stained blood vessels and cells were counted and quantified. \*\* $P < 0.01$ . Error bars indicate SEM ( $n = 3$ ).

cells.<sup>14</sup> Vimentin is a major intermediate filament expressed in fibroblasts, which constitutes cytoskeletal systems in eukaryotic cells. It has long been considered as a driving force of cell strength and tissue integrity.<sup>18</sup> To test the effect of miR-378a on

vimentin expression in the NIH/3T3 fibroblasts, a pair of luciferase reporter, which contained a fragment of the miR-378a binding site or a mutated counterpart, was developed (**Figure 4a**, upper panel). We confirmed that miR-378a transfection

decreased luciferase activity, while such effect was abolished when the binding sites were mutated or additional miR-Pirate378a was added (Figure 4a, lower panel). As a result, the expression of vimentin was elevated in miR-Pirate378a transfected fibroblasts (Figure 4b, upper panel). We then transfected NIH/3T3 cells with siRNAs (small interfering RNAs) against vimentin and confirmed the silencing of vimentin (Figure 4b, lower panel). Knockdown of vimentin inhibited cell adhesion (Figure 4c, Supplementary Figure S2a) and decelerated migration (Figure 4d, Supplementary Figure S2b), when compared with vector-transfected cells. Moreover, a lower velocity of migration of the siRNA-transfected cells was observed in the transwell assay (Figure 4e, Supplementary Figure S2c).

To confirm the effects of vimentin on mediating miR-378a-5p functions, we transfected NIH/3T3 fibroblasts with a vimentin expression construct. Overexpression of vimentin was confirmed through Western blot analysis (Figure 4f, left panel), which led to increased cell adhesion (Figure 4f, right panel) and migration (Figure 4g, Supplementary Figure S2d). We also found that over-expression of vimentin increased cell migration in the transwell assay (Figure 4h, Supplementary Figure S2e) and promoted cell differentiation (Figure 4i, Supplementary Figure S2f). Interestingly, the levels of vimentin increased drastically in the differentiated NIH/3T3 cells (Figure 4j, left panel), which was in accordance with the decrease in miR-378a levels (Figure 4j, right panel).

### Integrin beta-3 is a target of miR-378a-5p

By using an overlapping analysis of three miRNA target prediction algorithms (Pictar, TargetScan, and MiRBase), *in silico* analysis revealed integrin beta-3 as a miR-378a target (Supplementary Figure S3a). Integrin beta-3 is an integral cell surface protein which participates in cell adhesion and signal transduction. Dysregulation of integrin beta-3 has been linked to impaired endothelial cell migration.<sup>22</sup> To exploit the role of integrin beta-3 in wound healing, we tested the targeting of integrin beta-3 by generating a luciferase reporter construct containing a fragment of the integrin beta-3 3'-untranslated region and a mutant construct (Figure 5a). NIH/3T3 cells were cotransfected with miR-378a/miR-Pirate378a plasmid and one of the constructs. There was a decrease in luciferase activity in the cells transfected with the integrin beta-3 3'-untranslated region construct, but this inhibitory effect was abolished when the miR-378a binding sites were mutated or when the cells were cotransfected with miR-378a and miR-Pirate378a (Figure 5a).

Western blot analysis confirmed that transfection with miR-Pirate378a in NIH/3T3 fibroblasts increased integrin beta-3 expression (Figure 5b, left upper panel), which promoted VEGF expression (Figure 5b, left lower panel). Integrin beta-3 has been implicated in angiogenesis through stimulation of vascular endothelial growth factor (VEGF) expression, thus increasing neovascularization.<sup>23</sup> Consistent with these findings, we found that VEGF expression was elevated in the miR-Pirate378a-transfected cells. To test the effect of integrin beta-3 on cell activities, we employed an siRNA approach. Western blot analysis showed that expression of integrin beta-3 decreased when the cells were transfected with siRNA against integrin

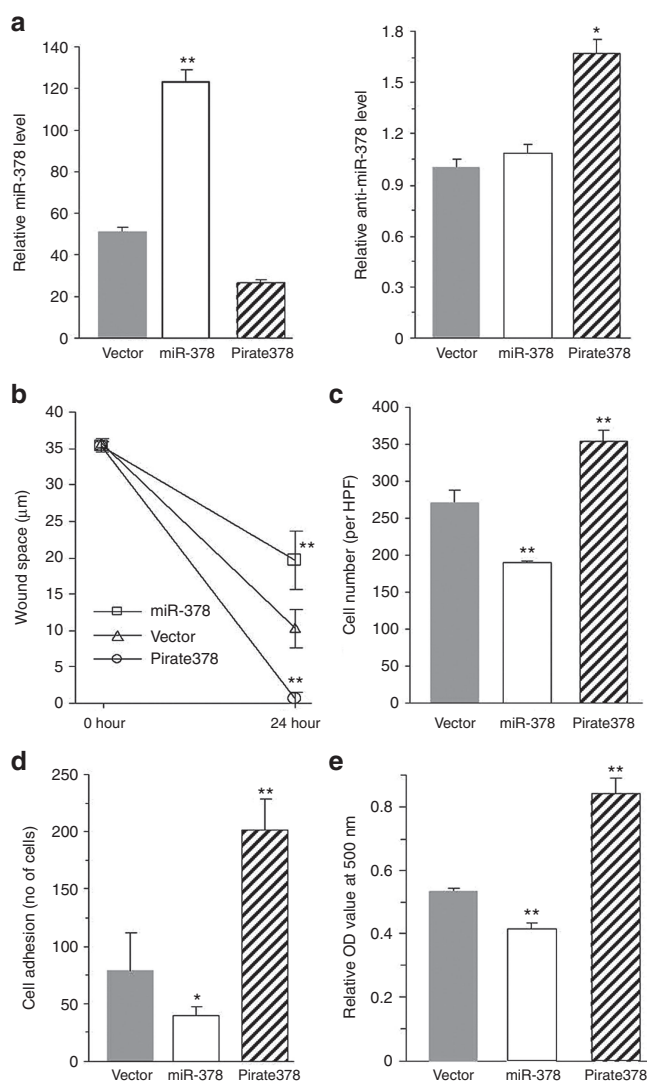


**Figure 3** Expression of miR-Pirate378a increases cell migration and adhesion. **(a)** Total RNAs isolated from NIH/3T3 cells transfected with miR-378a, miR-Pirate378a, or mock control, were analyzed by real-time PCR to confirm increased expression of mature miR-378a-5p and miR-Pirate378a in miR-378a-, and miR-Pirate378a-transfected cells, respectively. **(b)** Scratch wound healing test was applied to detect motility of transfected NIH/3T3 cells. Overexpression of miR-Pirate378a increased cell migration while overexpression of miR-378a-5p inhibited cell motility.  $**P < 0.01$ . Error bars indicate SEM ( $n = 3$ ). **(c)** Transwell migration test was applied to detect motility of NIH/3T3 cells in three-dimensional environment. Quantification of migrated cells showed that there were more miR-Pirate378a-transfected cells migrated through the membrane than the other two groups. **(d)** NIH/3T3 cells were incubated on Petri-dish for 2 hours to test adhesion. Fewer miR-378a cells adhered while more miR-Pirate378a cells adhered than the control.  $*P < 0.05$ . Error bars indicate SEM ( $n = 3$ ). **(e)** NIH/3T3 cells were induced to differentiate and subject to Oil-Red-O staining. Cell lysate prepared from differentiated NIH/3T3 cells were analyzed with optic density (OD) absorbance. There was higher OD reading in miR-Pirate378a group.

beta-3 (Figure 5b, right upper panel), which led to decreased VEGF expression (Figure 5b, right lower panel).

As a transmembrane receptor, integrin beta-3 mediates cell-cell and cell-extracellular matrix interaction.<sup>24</sup> We found that silencing integrin beta-3 led to impaired both cell invasion, as



might rescue the inhibitory effects of miR-378a on cell migration, and invasion.

### MiR-Pirate378a enhanced wound healing

We then confirmed that both vimentin and integrin beta-3 were targets of miR-378a. The levels of vimentin and integrin beta-3 in NIH/3T3 cells were analyzed by confocal microscopy. As expected, increased levels of vimentin and integrin beta-3 expression were observed in the miR-Pirate378a-transfected cells, while they were decreased in miR-378a-transfected cells (Figure 6a). Their expression levels were also examined in tissue samples obtained from the wound healing assay. Compared to wild-type mice, miR-Pirate378a transgenic mice showed higher expression levels of vimentin and integrin beta-3 around the wound area (Figure 6b).

Our finding that downregulation of endogenous miR-378a could facilitate tissue repair led us to exploit its therapeutic application. Several studies have demonstrated the utility of knocking-down of miRNAs by using anti-miRNA molecules *in vivo*.<sup>25,26</sup> By loading anti-miRNA oligo into PEG-conjugated gold nanoparticles as indicated (Supplementary Figure S3e), we were able to administrate a single dose of miR-Pirate378a to the adjacent wound area by intradermal injection. We found that nanoparticle treatment significantly reduced open wound areas over the course of 2–4 day treatments in wild type CD-1 mice (Figure 6c). Compared to the wounds on the left of the neck which were treated with blank vector loaded nanoparticles, miR-Pirate378a treatment (right side) showed a narrowed size and better healing (Figure 6d).

## DISCUSSION

We reported a novel transgenic anti-miRNA mouse model used to study tissue regeneration. We demonstrated that the knockdown of miR-378a by an endogenous, integrated antisense approach increased the expression of its targeted proteins, vimentin, and integrin beta-3, which accelerated fibroblast migration and differentiation *in vitro* and enhanced wound healing *in vivo*.

Various attempts have been made to silence miRNA *in vivo*. However, successfully delivering anti-miRNA fragments into

mammalian cells remains a challenge. Genetically modified mice offer insight into the constitutive repression of individual miRNAs. miRNAs contain highly conserved seed regions, which could be identical among different paralogs. These miRNAs are believed to exert similar functions through their common seed regions, which could target similar mRNAs. Therefore, the effects of knocking-out single miRNA could be jeopardized by other paralogs which target the same mRNAs. The anti-miRNA construct used in this study diminishes such influence from other miRNAs by binding the central loop of the miRNA precursor in addition to the seed region. Thus, this approach can be used to specifically knock down an individual member from a miRNA cluster. With highly matched sequences, this homological antisense transcript can sufficiently block the downstream processing of specific precursor miRNAs, thus preventing them from becoming functional. Also, the sixteen copies of the anti-miRNA sequence in the vector result in amplified silencing of the targeted miRNA.

miRNAs have recently emerged as key regulators of physical homeostasis. The regulatory network consisting of miRNAs and their targets maintain a stable internal environment. Any changes in homeostasis activate this regulatory network, leading to modification of gene expression. In this study, we found that the downregulation of miR-378a did not cause any apparent changes in the phenotype of transgenic mice (data not shown), but displayed a function during wound healing. These findings highlight the possibility that miRNAs are integrated into a complex network which maintains normal physiological conditions, while their dysregulations in response to intrinsic or extrinsic stimulations could result in pathophysiological dysfunction.<sup>27</sup> Recent findings illuminated the important role of miRNAs in wound healing. For example, miR-210 was found to be elevated in ischemic wounds, where hypoxia inducible factor-1 $\alpha$  (HIF-1 $\alpha$ ) was stabilized, and this accounted for attenuated keratinocyte proliferation and impaired wound reepithelization.<sup>28</sup>

Wound healing is achieved by complex physiological processes: monocytes and neutrophils are responsible for immune reaction, keratinocytes regenerate cutaneous epithelial cover, and fibroblasts exert contractile forces between cell–cell and cell–extracellular matrix junctions.<sup>29</sup> It also varies among species,

**Figure 4** MiR-378a-5p targets vimentin. **(a)** Upper panel: computational analysis showed that vimentin is a target of miR-378a. Constructs containing mutated/unmutated binding sites of vimentin were generated for luciferase assay. Lower panel: NIH/3T3 cells were co-transfected with miR-378a (Mi378) and luciferase reporter constructs (Luc-Vim) or the mutant (Luc-mut). The luciferase reporter vector (Luc) and the vector harboring a non-related region (G3R) were used as controls. MiR-378a repressed the activity of reporter with normal binding sites but had no effect on that with mutated binding sites. Moreover, transfection of miR-Pirate378a construct (Pi378) reversed the effect of miR-378a on vimentin, Error bars, SD ( $n = 3$ ). **(b)** Upper panel: cell lysates prepared from NIH/3T3 cells were subject to Western blot analysis. Transfection of miR-Pirate378a plasmid increased the expression of Vimentin. Lower panel: transfection of siRNA against vimentin decreased its level. **(c)** Adhesion test was applied to NIH/3T3 cells transiently transfected with siRNA against Vimentin or a control oligo. There were fewer cells adhered in siRNA group than that in the control group. **(d)** NIH/3T3 cells transiently transfected with siRNA against vimentin or a control oligo were subject to scratch wound healing test. Down-regulation of vimentin resulted in a lower migration rate in NIH/3T3 cells. **(e)** Transwell invasion test was applied to detect motility of NIH/3T3 cells in three-dimensional way. After Coomassie blue staining, quantification of migrated cells showed there were more NIH/3T3 cells in control group migrated through membrane than the cells transfected with siRNA against vimentin. **(f)** Left panel: cell lysates prepared from NIH/3T3 cells were subject to Western blot analysis. Transfection of vimentin expression construct increased its level. Right panel: adhesion test was applied to NIH/3T3 cells transiently transfected with vimentin expression construct or the control vector. There were more cells adhered in vimentin overexpression group than that in the control group. **(g)** NIH/3T3 cells transiently transfected with vimentin expression construct or the control vectors were subject to scratch wound healing test. Overexpression of vimentin increased cell motility. **(h)** Transwell migration test was applied to NIH/3T3 cells transiently transfected with vimentin expression construct or the control vector. There were more cells migrated through membrane in vimentin rescue group than that in the control group. **(i)** NIH/3T3 cells transiently transfected with vimentin expression construct or the control vectors were subject to oil red staining. There were more differentiated cells in vimentin overexpression group. **(j)** Left panel: NIH/3T3 cells were induced to differentiate and subject to western blot analysis. Differentiated cells increased expression of vimentin. Right panel: differentiated cells had decreased levels of mature miR-378a.

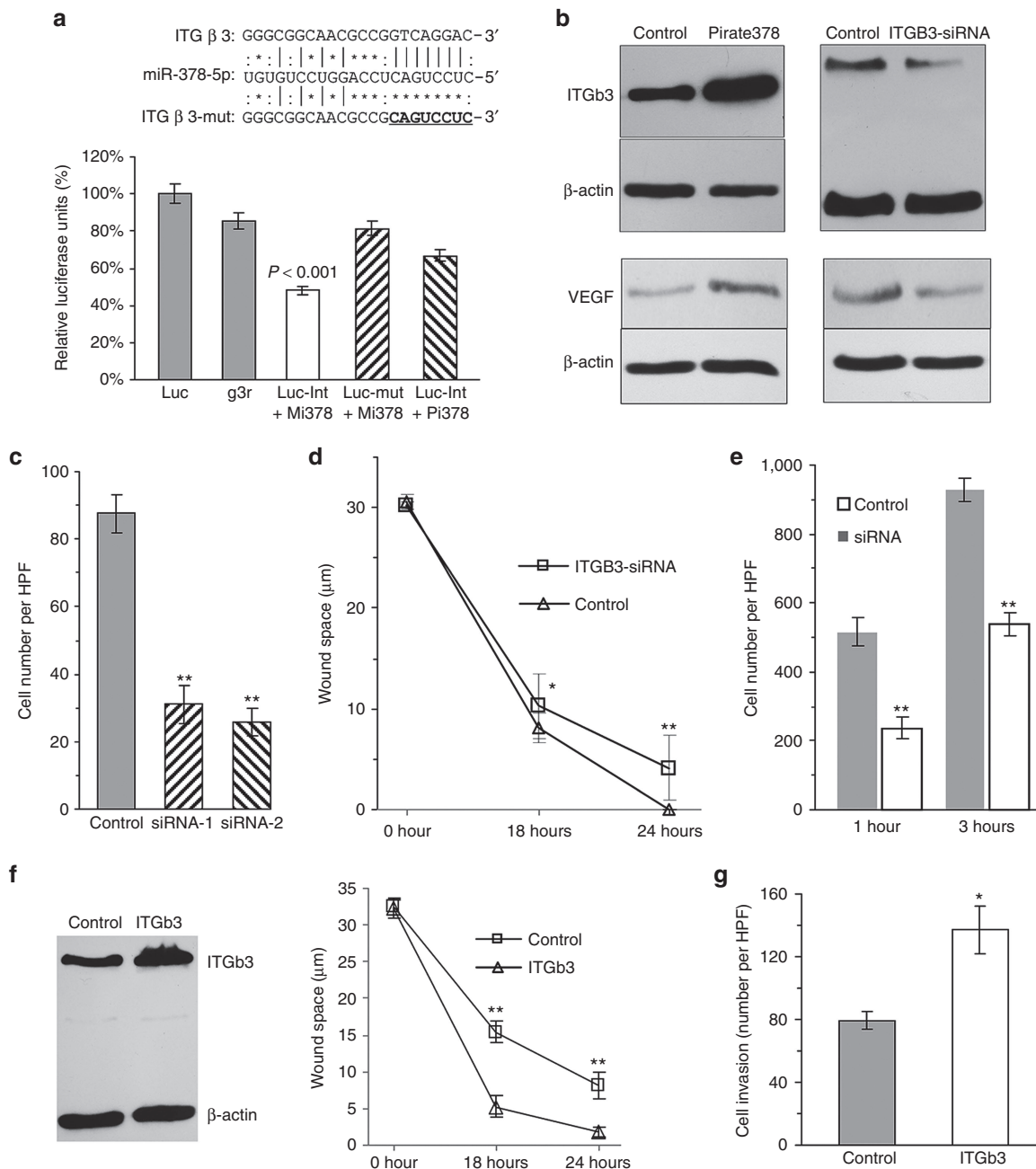


**Figure 5** MiR-378a-5p targets integrin beta-3. **(a)** Upper panel: computational analysis showed that integrin beta-3 was a potential target of miR-378a. Constructs containing mutated/unmutated binding sites of integrin beta-3 were generated for luciferase assay. Lower panel: NIH/3T3 fibroblasts were co-transfected with miR-378a (Mi378) and luciferase reporter constructs (Luc-Int) or the mutants (Luc-mut). The luciferase reporter vector (Luc) and the vector harboring a non-related region (G3R) were used as controls. MiR-378a repressed the activity of the constructs containing the target sites, which was reversed when the target sites were mutated. Cotransfection with the luciferase construct and miR-Pirate378 (Pi378) also reversed the inhibitory effect. **(b)** Cell lysates prepared from NIH/3T3 cells were subject to Western blot analysis. Left panel: transfection of miR-Pirate378a plasmid increased the expression of integrin beta-3 and VEGF. Right panel: transient transfection of siRNA targeting integrin beta-3 decreased levels of integrin beta-3 and VEGF. Endogenous beta-actin was served as loading control. **(c)** Transwell migration test was applied to NIH/3T3 cells transiently transfected with two siRNAs against integrin beta-3 or a control oligo. There were fewer cells migrated through membrane in the siRNA groups than that in the control group. **(d)** NIH/3T3 cells transiently transfected with siRNA against integrin beta-3 or a control oligo were subject to scratch wound healing test. Down-regulation of integrin beta-3 inhibited cell migration. **(e)** Adhesion assay was performed on NIH/3T3 cells transiently transfected with siRNAs against integrin beta-3 or a control oligo. There were less cells adhered in siRNA groups than that in the control group. **(f)** Transfection of integrin beta-3 construct increased integrin beta-3 expression. Right panel: upregulation of integrin beta-3 increased cell migration compared to control oligo. **(g)** Transwell migration test was performed and showed that more NIH/3T3 cells transfected with integrin beta-3 construct migrated through Matrigel (BD Biosciences, Mississauga, Ontario, Canada).

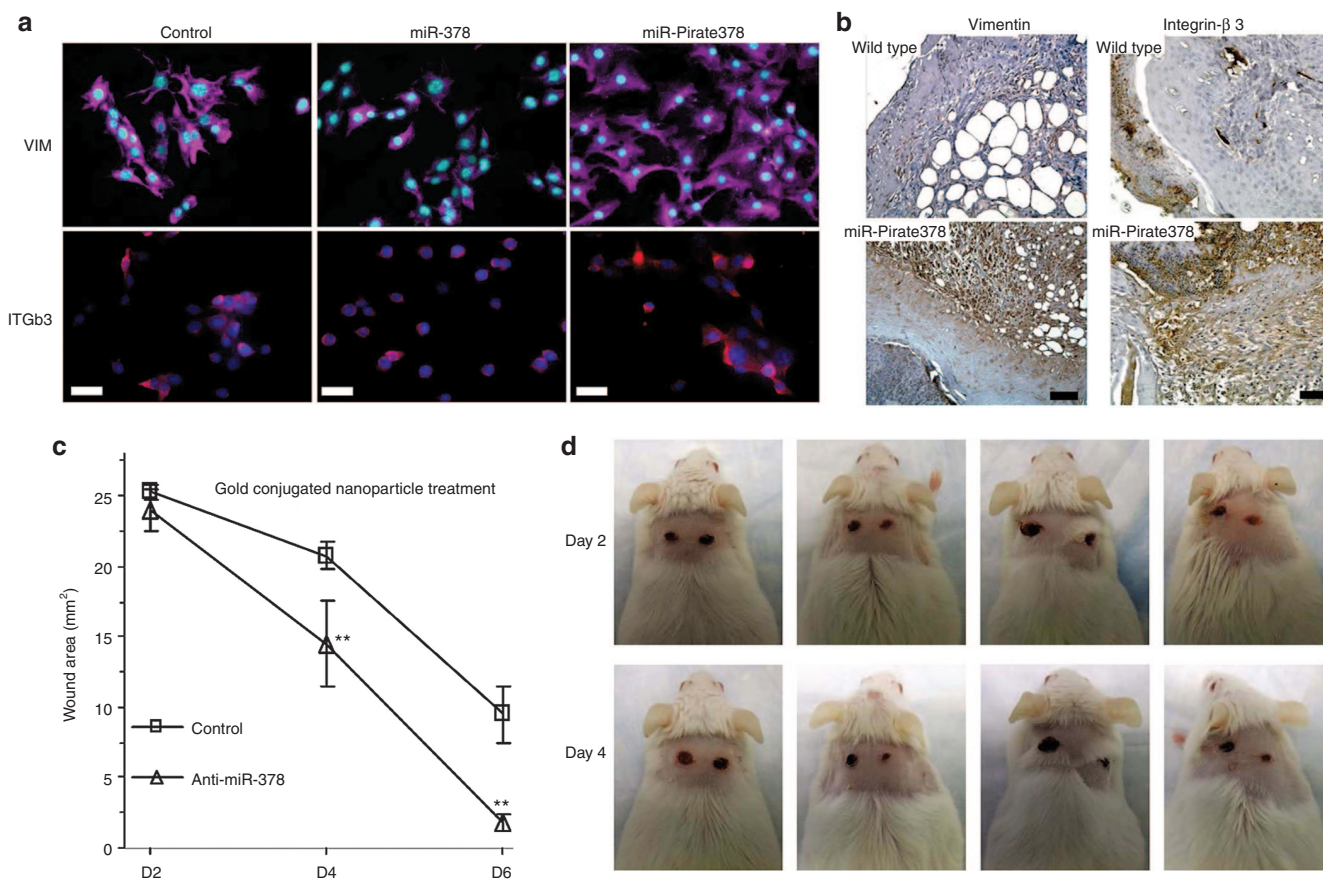


**Figure 6** Effects of miR-Pirate378a on expression of vimentin and integrin beta-3 and wound repair. **(a)** NIH/3T3 fibroblasts stably transfected with miR-378a, miR-Pirate378a expression plasmid, or mock control were subject to confocal microscopic analysis. Vimentin and integrin beta-3 were downregulated in miR-378a transfected cells but upregulated in miR-Pirate378a-transfected cells compared to the control. Scale bar = 50  $\mu$ m. **(b)** Immunohistochemistry analysis indicated that expressions of vimentin and integrin beta-3 increased in miR-Pirate378a transgenic mice compared to wild type mice. Scale bar, 50  $\mu$ m. **(c)** Wide-type CD1 mice were treated with miR-Pirate378a conjugated to gold nanoparticles. Compared to blank control, treatment with miR-Pirate378a nanoparticle enhanced wound healing ( $n = 3$ ,  $**P < 0.01$ ). **(d)** Picture taken from the second and the fourth days showed that miR-Pirate378a nanoparticle treatment had enhanced wound healing (right side) compared with blank control (left side).

for example, human wound healing predominantly relies on reepithelization while wound contraction is more important in mice.<sup>30</sup> This is why we chose mouse fibroblasts in studying wound contraction *in vitro*. We observed that miR-Pirate378a contributed to fibroblast migration in cultured NIH/3T3 cells, which was due to elevated expression of vimentin and integrin beta-3. It has been reported that vimentin is required to generate traction forces during wound healing, and also that vimentin-deficient mice showed impaired wound healing.<sup>18</sup> Comparatively, integrin beta-3 is an integral cell-surface protein which participates in cell adhesion as well as bidirectional signal transmission. It has been shown that the inhibition of integrin beta-3 expression in endothelial cells resulted in impairment of cell migration.<sup>22</sup> Moreover, by interplaying with VEGF signaling, integrin beta-3 has been shown to control tumor growth through the promotion of tumor vascularization.<sup>23</sup> In this study, we observed that elevated levels of vimentin and integrin beta-3 contributed to accelerated fibroblasts migration, which is critical in the early stage of wound healing.<sup>31</sup>

We also discovered enhanced differentiation in NIH/3T3 cells transfected with miR-Pirate378a. Interestingly, during the process of differentiation, expression of vimentin was evoked, which

underlined the importance of vimentin in fibroblast differentiation. Since vimentin is targeted by miR-378a, it highlights the role of miR-Pirate378a in inducing cell differentiation by rescuing vimentin expression. When NIH/3T3 cells were originally obtained by Green *et al.* from mouse cells, they found that NIH/3T3 cells had the potential to differentiate into adipose cells.<sup>21</sup> Herein, we took advantage of this to detect the differentiation capacity of NIH/3T3 cells. We demonstrated that expression of miR-Pirate378a promoted adipogenesis by upregulation of vimentin expression. Although the intricate mechanism of wound healing is not completely understood, adipocytes and adipose-derived cells have been regarded as important mediators in tissue regeneration.<sup>32</sup> Furthermore, we found that the levels of mature miR-378a decreased in differentiated NIH/3T3 cells, which was in agreement with increased vimentin expression upon differentiation. Finally, we confirmed the increased differentiation of myofibroblasts in tissue samples, as we detected higher levels of alpha-smooth muscle actin expression in the miR-Pirate378a transgenic mice during wound healing.

The process of wound healing requires epithelial cell regeneration and proliferation. However, we did not detect any difference in BrdU and Ki67 expression. We also assessed the proliferation

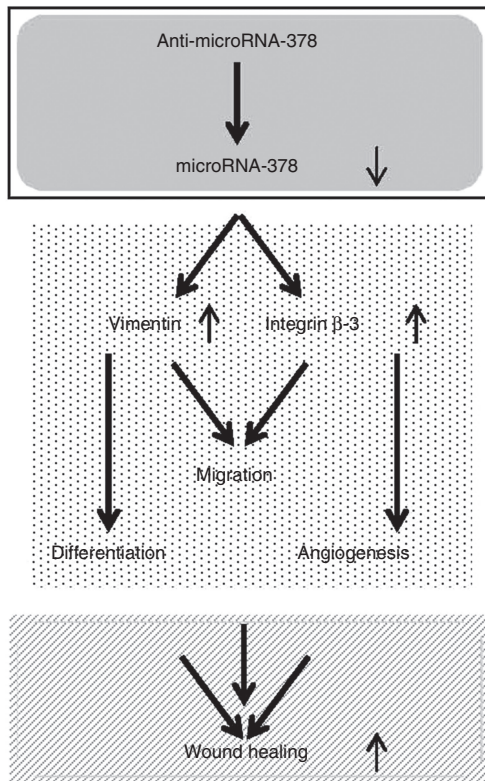


**Figure 7 Summary of the results.** Flow chart is showing miR-378 regulates wound healing by mediating multiple pathways.

of NIH/3T3 cells *in vitro*, which showed little difference between miR-378a- and miR-Pirate378a-transfected cells (data not shown). This might be due to the overall activation of cellular regeneration mechanism, which leads to a fast growing pace of epithelial cells in both the control and experimental groups. Notably, we found that the overexpression of integrin beta-3 promoted tube-like structure formation *in vitro* and angiogenesis *in vivo*, probably through the activation of VEGF signaling. These findings suggest that miR-378a regulates single physical process (wound healing) by interfering with multiple pathways (cell migration, differentiation, and angiogenesis, **Figure 7**).

In summary, we have shown a novel wound healing model in miR-Pirate378a transgenic mice. The investigation of miRNA in regulating tissue repairing can open up vast opportunities. Further diabetic animal models could be developed based on our current transgenic mice, and more clinically oriented research could be performed. Collectively, our data have shown that targeting miR-378a could accelerate wound healing in a murine model. Our novel approach to miRNA inhibition adds a new layer of knowledge in this area and warrants further investigation.

## MATERIALS AND METHODS

**Construct generation.** The design of miR-378a expression plasmid was described previously.<sup>3</sup> In brief, two human pre-miR-378a units were inserted into a mammalian expression vector pEGFP-N1 driven by an H1 promoter, between the restriction enzyme sites BglII and HindIII (**Figure 1a**). To suppress the expression and function of endogenous miR-378a, we generated a construct that produced RNA transcripts containing 16 repeats. Each repeat can play two functional roles. (i) It can interfere with normal processing of endogenous miR-378a, producing imperfect

truncated miR-378a. (ii) It can bind and arrest the functions of endogenous mature miR-378a-5p, which were processed through the normal miRNA biogenesis pathway. Since the RNA transcript could interact with up to 16 miRNAs, it can form large complexes with miRNAs and thereby arrest the functions of the mature miR-378a-5p. The construct was named *miR-Pirate378a*, meaning *miRNA-interacting RNA—Producing imperfect RNA and tangling endogenous miR-378a (miR-Pirate)*. The miR-Pirate378a transcript could bind and block miR-378a-5p function.

For luciferase assay, two pairs of primers were used to clone the fragments of each binding site and its mutant control. The PCR products were then digested with SacI and MluI and inserted into a SacI- and MluI-digested pMir-Report vector (Ambion, Life Technologies, Burlington, Ontario, Canada), producing a luciferase construct and a mutant counterpart.<sup>33</sup> The vimentin luciferase constructs and expression construct was described previously.<sup>14</sup> The integrin beta-3 luciferase construct was generated with mu-integrinβ3-R378-SacI and mu-integrinβ3-R378. Combination with mu-integrinβ3-R378-MluI-mut generated mutations at the miR-378a-5p-binding sites. All the primers' sequences are listed in Supplementary Information (**Supplementary Figure S1a**). The integrin beta-3 cDNA was a generous gift of Dr Ni from St. Michael's Hospital (Toronto).

**Generation of transgenic mice and wound healing experiment.** An anti-miR-378 sponge was generated by digestion of anti-miR-378 plasmid with BglII and StuI. The transgene fragment was then purified from agarose gel electrophoresis and suspended at a concentration of 2 ng/μl. Transgenic anti-miR-378 mouse strains were developed by microinjection of anti-miR-378 sponge into fertilized zygotes of CD-1 mouse. Injected eggs were then implanted into oviduct of female mouse. Transgenic strains were maintained by backcrossing with CD-1 mouse.<sup>14,16</sup> Hemizygous positive transgenic mice were selected by genotyping. And homozygous negative mice derived from same founders were used as controls. At 4 weeks of age, 10 transgenic and 10 wild-type control mice were subject to skin biopsy using a punch (Miltek, York, PA) of 5 mm in diameter. A pair of full-thickness, excisional wounds were created on the dorsal region of each mouse. Wound size was measured by multiplying longest length by greatest width, and all mice were killed on the seventh day. Tissue samples were collected for further study. All of the methods were performed following a protocol approved by the Animal Care Committee of Sunnybrook Research Institute.

**Immunoreaction assay.** Immunoreaction assay was performed as previously described.<sup>34</sup> Western blot and immunohistochemistry assay were conducted by using antibodies against vimentin (Cell Signaling, Danvers, MA) and integrin beta-3 (Santa Cruz Biotechnology, Dallas, TX). Bromodeoxyuridine (BrdU) (BD Pharmingen, Mississauga, Ontario, Canada) was used to label cell proliferation *in vivo*. Mice were injected with 1 mg BrdU solution intraperitoneally 12 hours before killing. Antibody against BrdU (Biosdesign, Tempe, AZ) was used to detect cellular incorporated BrdU in immunohistochemistry assay. Anti-CD34 antibody (Santa Cruz Biotechnology) was used to probe blood vessel density in tissue samples and anti-VEGF antibody (BD Biosciences) was used for Western blotting.

Wound tissue samples were freshly fixed in 10% neutral buffered formalin overnight, and embedded in paraffin. Vertical section through the center of wound was conducted by microtome (Leica RM2255; Leica Microsystems, Concord, Ontario, Canada). Immunoreaction assay was performed as previously described.<sup>34</sup> Quantification of Ki67/BrdU was performed by ImageJ software (NIH, Bethesda, MD). In brief, 20 stained tissue sections were scanned initially under the low objective to select the suitable fields that accurately represent the density and distribution of positive staining. Positively stained cells were seen in the basal region of epithelium. Four pictures were taken from each slide. A total 80 images were analyzed using a color subtractive technique, as previously described.<sup>33</sup>

For immunostaining of vimentin and integrin beta-3, the percentage of positive tumor cells was assigned as follows: 1 (up to 25% of positive cells), 2 (25–50% of positive cells), 3 (50–75% of positive cells) and 4 (more than 75% of positive cells). Intensity scores ranged from 0 to 3: 0,

no staining; 1, weak staining; 2, moderate staining, and 3, strong staining. Multiplication of the two scores resulted in a final score ranging from 0 to 12. Twenty samples were scored on the grading system with score 0–6 defined as low expression and score 8–12 defined as high expression.

**Cell culture.** Mouse fibroblast cell line NIH/3T3 (CRL-1658) was cultured in Dulbecco's Modified Eagle's Medium (DMEM) supplemented with 10% bovine calf serum, penicillin (100 U/ml) and streptomycin (100 U/ml). G418 (500 µg/ml) was added into culture media after cells were transfected with plasmids. Endothelial cell line YPEN-1 (CRL-2222) was cultured in Iscove's Modified Dulbecco's Media (IMDM) media supplemented with 10% fetal bovine serum, penicillin (100 U/ml) and streptomycin (100 U/ml). Cells were maintained in a humidified incubator containing 5% CO<sub>2</sub> at 37 °C.

**Confocal microscopy.** NIH/3T3 cells were fixed with 4% paraformaldehyde in phosphate-buffered saline (PBS) for 30 minutes, and then permeabilized with 0.1% Triton-X-100 for 20 minutes at room temperature. After blocking with 10% goat serum for 60 minutes, primary antibody against vimentin and integrin beta-3 were applied at a concentration of 1:200 and 1:100, respectively. Cy5- or FITC-conjugated goat antimouse secondary antibodies (Jackson ImmunoResearch, West Grove, PA) were then incubated for 1 hour and subject to fluorescence confocal microscopy examination (Zeiss Axiovert, Carl Zeiss Microscopy, Berlin, Germany).

**Cell adhesion test.** In cell adhesion assay, NIH/3T3 cells were incubated on Petri dish at a density of  $1 \times 10^6$  cells/well. Images were taken in a consequent time points at 0, 2, and 4 hours to test adhesion ability.

**Cell migration test.** Cell migration was tested by scratch assay and transwell assay. In the scratch assay, NIH/3T3 cells were plated in six-well plates at a density of  $1 \times 10^6$  cells/well for 12 hours. To diminish the influence of proliferation, the cells were treated with Mitomycin C (Sigma-Aldrich, St. Louis, MO) at 10 µg/ml for 2 hours before being changed to serum-free media. The cultures were then scraped linearly with micropipette tips (BioMart, Toronto, Ontario, Canada). Cell migration patterns were recorded by light microscopy at 0, 18, and 24 hours. Migrated distance was measured and quantified. To detect cell motility in a three-dimensional way, transwell chambers (Coster, Sigma-Aldrich) were placed in 24-well tissue culture dish and  $1 \times 10^5$  of cells with 100 µl media were loaded into the upper chamber of the transwell. The lower chamber was filled with 600 µl DMEM containing 10% fetal bovine serum. After 12-hour incubation at 37 °C, nonmigrated cells were removed with a cotton swab and invaded cells were stained with Coomassie brilliant blue (Bio-Rad, Hercules, CA) for 5 minutes. Photos were taken under a light microscope (Zeiss, Carl Zeiss Microscopy).

**Cell differentiation assay.** NIH/3T3 cells were grown to confluence in DMEM supplemented with 10% fetal bovine serum for 2 days. MDI (MIX, Dex, Insulin) induction media was prepared by adding 1% Isobutylmethylxanthine (Sigma-Aldrich), 0.1% Dexamethasone (Sigma-Aldrich) and 0.1% insulin (Lilly, Eli Lilly Canada, Toronto, Ontario, Canada) into DMEM media with 10% fetal bovine serum. NIH/3T3 cells were stimulated with MDI media for 7 days before being replaced by DMEM media supplemented with 0.1% insulin (Lilly). Differentiated cells were subject to Oil-Red-O staining.

**Oil-Red-O staining.** Differentiated NIH/3T3 cells were washed twice with PBS before incubation in 10% formalin for 2 hours. Cells were washed with 60% isopropanol for 5 minutes and dried at room temperature. About 1 ml of Oil-Red-O solution (Sigma-Aldrich) was then added and incubated for 10 minutes. Images were captured by light microscopy after washing with distilled water. To measure the optical density, cells were washed with 1 ml of 100% isopropanol and the optical density was recorded at 500 nm using isopropanol as control.

**Real-time PCR.** Total RNA from  $1 \times 10^6$  cells or ~0.05 g tissues was extracted by using mircury RNA isolation kit (Exiqon, Vedbaek, Denmark). Reverse

transcript PCR was performed by using miscript II RT kit (Qiagen, Toronto, Ontario, Canada). Mature miR-378a levels were measured using SYBR green PCR kit (Qiagen) in real-time PCR (Applied Biosystems, Life Technologies, Burlington, Ontario, Canada) as described.<sup>35,36</sup> We designed primers Pre-miR378F and Pre-miR378R to detect endogenous miR-378a precursor, has-miR-378 to detect mature miR-378a-5p, miR-378N, and miR-378C to detect expression of the precursor of ectopic transfected miR-378a, miR-378N, and anti-mir-378 to detect expression of miR-Pirate378a, and miR378-truncated to detect expression of the mature miR-Pirate378s-5p. Primers used as controls were mo-Gapdh1F and mo-Gapdh250R (for mouse tissues).

**Luciferase activity assay.** NIH/3T3 cells were seeded onto 12-well tissue culture dishes at a density of  $1 \times 10^5$  cells/well. The cells were cotransfected with the luciferase reporter constructs and miR-378a/miR-Pirate378a plasmid, using Lipofectamine 2000. Firefly reporter plasmids (Ambion, Life Technologies) with or without an unrelated fragment insert (G3R) served as positive controls. After 12 hours, cell lysate was prepared by using Dual-Luciferase Reporter Assay Kit (Promega, Madison, WI) and luciferase activity was detected by luminescence counter (Perkin Elmer, Waltham, MA) as previously described.<sup>37</sup>

**Nanoparticle synthesis and delivery.** For synthesis of anti-miR-PEG conjugate, 20 nmol thiol modified miR-Pirate378a fragments (GenePharma, Shanghai, China) were dissolved in 800 µl of RNase-free water. The mPEG-SH (PG1-TH-2k, Nanocs, New York, NY) were mixed with the miR-Pirate378a fragments at a 1:20 molar ratio. Then 10 nm gold nanoparticles (Cytodiagnosics, Burlington, Ontario, Canada) were mixed with 1 µg anti-miR-PEG at weight ratio of 1:1 for conjugation. The mixture was gently shaken at 60 °C for 30 minutes and transferred into a syringe. Upon wounding by skin punch, the nanoparticles with miR-Pirate378a or blank control were administered intradermally in a volume of 100 µl as previously described.<sup>38</sup>

**Statistical analysis.** All experiments were performed in triplicate and numerical data were subject to independent sample *t* test. The levels of significance were set at \**P* < 0.05 and \*\**P* < 0.01.

## SUPPLEMENTARY MATERIAL

**Figure S1.** Effects of miR-378a on cell activities.

**Figure S2.** Effects of vimentin on cell activities.

**Figure S3.** Effects of integrin beta-3 on cell activities.

## ACKNOWLEDGMENTS

The authors thank Weining Yang for assistance in writing the paper. This work was supported by grants from Canadian Institutes of Health Research (MOP-102635, MOP-111171) and a Discovery Grant from the Natural Sciences and Engineering Research Council of Canada (NSERC; 227937-2012) to B.B.Y. who is the recipient of a Career Investigator Award (CI 7418) from the Heart and Stroke Foundation of Ontario. H.L. is a recipient of the Connaught International Student Award. L.C. is supported by an award from Summer Undergraduate Research Program, Institute of Medical Science, University of Toronto. H.L. performed and coordinated the project. W.W.D. was involved in wound healing assay. L.C. helped some cell migration assays. S.G. and A.K. were involved in RNA analysis. H.L. and B.B.Y. designed the project and analyzed the results. H.L. and B.B.Y. wrote the paper. All authors declare no conflict of interest for the study.

## REFERENCES

- Banerjee, J and Sen, CK (2013). MicroRNAs in skin and wound healing. *Methods Mol Biol* **936**: 343–356.
- Roy, S and Sen, CK (2012). miRNA in wound inflammation and angiogenesis. *Microcirculation* **19**: 224–232.
- Lee, DY, Deng, Z, Wang, CH and Yang, BB (2007). MicroRNA-378 promotes cell survival, tumor growth, and angiogenesis by targeting SuFu and Fus-1 expression. *Proc Natl Acad Sci USA* **104**: 20350–20355.
- Rutnam, ZJ, Wight, TN and Yang, BB (2013). miRNAs regulate expression and function of extracellular matrix molecules. *Matrix Biol* **32**: 74–85.
- Lee, DY, Jeyapalan, Z, Fang, L, Yang, J, Zhang, Y, Yee, AY *et al.* (2010). Expression of versican 3'-untranslated region modulates endogenous microRNA functions. *PLoS One* **5**: e13599.

6. Jeyapalan, Z, Deng, Z, Shatseva, T, Fang, L, He, C and Yang, BB (2011). Expression of CD44 3'-untranslated region regulates endogenous microRNA functions in tumorigenesis and angiogenesis. *Nucleic Acids Res* **39**: 3026–3041.
7. Rutnam, ZJ, Du, WW, Yang, W, Yang, X and Yang, BB (2014). The pseudogene TUSC2P promotes TUSC2 function by binding multiple microRNAs. *Nat Commun* **5**: 2914.
8. Yang, X, Rutnam, ZJ, Jiao, C, Wei, D, Xie, Y, Du, J *et al.* (2012). An anti-let-7 sponge decoys and decays endogenous let-7 functions. *Cell Cycle* **11**: 3097–3108.
9. Ebert, MS, Neilson, JR and Sharp, PA (2007). MicroRNA sponges: competitive inhibitors of small RNAs in mammalian cells. *Nat Methods* **4**: 721–726.
10. Boutla, A, Delidakis, C and Tabler, M (2003). Developmental defects by antisense-mediated inactivation of micro-RNAs 2 and 13 in *Drosophila* and the identification of putative target genes. *Nucleic Acids Res* **31**: 4973–4980.
11. Meister, G, Landthaler, M, Dorsett, Y and Tuschl, T (2004). Sequence-specific inhibition of microRNA- and siRNA-induced RNA silencing. *RNA* **10**: 544–550.
12. Davis, S, Lollo, B, Freier, S and Esau, C (2006). Improved targeting of miRNA with antisense oligonucleotides. *Nucleic Acids Res* **34**: 2294–2304.
13. Carè, A, Catalucci, D, Felicetti, F, Bonci, D, Addario, A, Gallo, P *et al.* (2007). MicroRNA-133 controls cardiac hypertrophy. *Nat Med* **13**: 613–618.
14. Deng, Z, Du, WW, Fang, L, Shan, SW, Qian, J, Lin, J *et al.* (2013). The intermediate filament vimentin mediates microRNA miR-378 function in cellular self-renewal by regulating the expression of the Sox2 transcription factor. *J Biol Chem* **288**: 319–331.
15. Kahai, S, Lee, SC, Lee, DY, Yang, J, Li, M, Wang, CH *et al.* (2009). MicroRNA miR-378 regulates nephronectin expression modulating osteoblast differentiation by targeting GalNT-7. *PLoS One* **4**: e7535.
16. Deng, Z, Yang, X, Fang, L, Rutnam, ZJ and Yang, BB (2013). Misprocessing and functional arrest of microRNAs by miR-Pirate: roles of miR-378 and miR-17. *Biochem J* **450**: 375–386.
17. Li, H and Yang, BB (2013). Friend or foe: the role of microRNA in chemotherapy resistance. *Acta Pharmacol Sin* **34**: 870–879.
18. Eckes, B, Colucci-Guyon, E, Smola, H, Nodder, S, Babinet, C, Krieg, T *et al.* (2000). Impaired wound healing in embryonic and adult mice lacking vimentin. *J Cell Sci* **113** (Pt 13): 2455–2462.
19. Shu, YY and Maibach, HI (2011). Estrogen and skin: therapeutic options. *Am J Clin Dermatol* **12**: 297–311.
20. Speight, P, Nakano, H, Kelley, TJ, Hinz, B and Kapus, A (2013). Differential topical susceptibility to TGFβ in intact and injured regions of the epithelium: key role in myofibroblast transition. *Mol Biol Cell* **24**: 3326–3336.
21. Green, H and Kehinde, O (1975). An established preadipose cell line and its differentiation in culture. II. Factors affecting the adipose conversion. *Cell* **5**: 19–27.
22. Mahabeleshwar, GH, Chen, J, Feng, W, Somanath, PR, Razorenova, OV and Byzova, TV (2008). Integrin affinity modulation in angiogenesis. *Cell Cycle* **7**: 335–347.
23. De, S, Razorenova, O, McCabe, NP, O'Toole, T, Qin, J and Byzova, TV (2005). VEGF-integrin interplay controls tumor growth and vascularization. *Proc Natl Acad Sci USA* **102**: 7589–7594.
24. Sakamoto, Y, Ogita, H, Komura, H and Takai, Y (2008). Involvement of nectin in inactivation of integrin alpha(v)beta(3) after the establishment of cell-cell adhesion. *J Biol Chem* **283**: 496–505.
25. Krützfeldt, J, Rajewsky, N, Braich, R, Rajeev, KG, Tuschl, T, Manoharan, M *et al.* (2005). Silencing of microRNAs *in vivo* with 'antagomirs'. *Nature* **438**: 685–689.
26. Babar, IA, Cheng, CJ, Booth, CJ, Liang, X, Weidhaas, JB, Saltzman, WM *et al.* (2012). Nanoparticle-based therapy in an *in vivo* microRNA-155 (miR-155)-dependent mouse model of lymphoma. *Proc Natl Acad Sci USA* **109**: E1695–E1704.
27. Rottiers, V and Näär, AM (2012). MicroRNAs in metabolism and metabolic disorders. *Nat Rev Mol Cell Biol* **13**: 239–250.
28. Biswas, S, Roy, S, Banerjee, J, Hussain, SR, Khanna, S, Meenakshisundaram, G *et al.* (2010). Hypoxia inducible microRNA 210 attenuates keratinocyte proliferation and impairs closure in a murine model of ischemic wounds. *Proc Natl Acad Sci USA* **107**: 6976–6981.
29. Hong, HJ, Jin, SE, Park, JS, Ahn, WS and Kim, CK (2008). Accelerated wound healing by smad3 antisense oligonucleotides-impregnated chitosan/alginate polyelectrolyte complex. *Biomaterials* **29**: 4831–4837.
30. Moulin, V, Auger, FA, Garrel, D and Germain, L (2000). Role of wound healing myofibroblasts on re-epithelialization of human skin. *Burns* **26**: 3–12.
31. Bavan, L, Midwood, K and Nanchahal, J (2011). MicroRNA epigenetics: a new avenue for wound healing research. *BioDrugs* **25**: 27–41.
32. Philips, BJ, Marra, KG and Rubin, JP (2012). Adipose stem cell-based soft tissue regeneration. *Expert Opin Biol Ther* **12**: 155–163.
33. Liu, F, Lv, Q, Du, WW, Li, H, Yang, X, Liu, D *et al.* (2013). Specificity of miR-378a-5p targeting rodent fibronectin. *Biochim Biophys Acta* **1833**: 3272–3285.
34. Li, H and Yang, BB (2012). Stress response of glioblastoma cells mediated by miR-17-5p targeting PTEN and the passenger strand miR-17-3p targeting MDM2. *Oncotarget* **3**: 1653–1668.
35. Fang, L, Du, WW, Yang, X, Chen, K, Ghanekar, A, Levy, G *et al.* (2013). Versican 3'-untranslated region (3'-UTR) functions as a ceRNA in inducing the development of hepatocellular carcinoma by regulating miRNA activity. *FASEB J* **27**: 907–919.
36. Yang, X, Du, WW, Li, H, Liu, F, Khorshidi, A, Rutnam, ZJ *et al.* (2013). Both mature miR-17-5p and passenger strand miR-17-3p target TIMP3 and induce prostate tumor growth and invasion. *Nucleic Acids Res* **41**: 9688–9704.
37. Rutnam, ZJ and Yang, BB (2012). The non-coding 3' UTR of CD44 induces metastasis by regulating extracellular matrix functions. *J Cell Sci* **125** (Pt 8): 2075–2085.
38. Steinstraesser, L, Hirsch, T, Beller, J, Mittler, D, Sorkin, M, Pazzierny, G *et al.* (2007). Transient non-viral cutaneous gene delivery in burn wounds. *J Gene Med* **9**: 949–955.



This work is licensed under a Creative Commons Attribution-NonCommercial-NoDerivs 3.0 Unported License. The images or other third party material in this article are included in the article's Creative Commons license, unless indicated otherwise in the credit line; if the material is not included under the Creative Commons license, users will need to obtain permission from the license holder to reproduce the material. To view a copy of this license, visit <http://creativecommons.org/licenses/by-nc-nd/3.0/>